doi:10.1038/nature05455

ARTICLES

Coupling substrate and ion binding to extracellular gate of a sodium-dependent aspartate transporter

Olga Boudker[1]*†, Renae M. Ryan[1]*†, Dinesh Yernool[1]†, Keiko Shimamoto[3] & Eric Gouaux[1,2]†

Secondary transporters are integral membrane proteins that catalyse the movement of substrate molecules across the lipid bilayer by coupling substrate transport to one or more ion gradients, thereby providing a mechanism for the concentrative uptake of substrates. Here we describe crystallographic and thermodynamic studies of Glt_{Ph}, a sodium (Na^+)-coupled aspartate transporter, defining sites for aspartate, two sodium ions and D,L-threo-β-benzyloxyaspartate, an inhibitor. We further show that helical hairpin 2 is the extracellular gate that controls access of substrate and ions to the internal binding sites. At least two sodium ions bind in close proximity to the substrate and these sodium-binding sites, together with the sodium-binding sites in another sodium-coupled transporter, LeuT, define an unwound α-helix as the central element of the ion-binding motif, a motif well suited to the binding of sodium and to participation in conformational changes that accompany ion binding and unbinding during the transport cycle.

Life depends on the coordinated movement of molecules and ions across the membranes of cells and organelles, catalysed by specific membrane proteins—channels and pumps. Channels create continuous transmembrane pores and facilitate the movement of ions and electrolytes down their electrochemical gradients[1]. In contrast, pumps couple the thermodynamically unfavourable movement of substrates to energy stored in the form of ATP or electrochemical gradients[2,3]. Secondary transporters are 'pumps' that couple movements of substrates and one or more ions and thus 'push' their substrates up steep thermodynamic hills by harnessing pre-existing ion gradients[4]. Sodium-driven secondary transporters are particularly important in biology, catalysing the uptake of neurotransmitters[5], sugars[6] and amino acids[4,7]. The mechanisms by which these transporters couple substrate and sodium transport are currently fundamental unanswered questions in biology.

Mammalian excitatory amino acid transporters (EAATs) catalyse the uptake of the neurotransmitter glutamate from chemical synapses[8] and are representatives of a large family of secondary transporters that move acidic and neutral amino acids, as well as dicarboxylic acids, across the membranes of prokaryotic and eukaryotic cells[9]. By coupling the neurotransmitter uptake to the co-transport of three sodium ions and one proton, and the countertransport of a potassium (K^+) ion, EAATs pump substrates against concentration gradients of up to several thousandfold[10–12]. The recently determined structure of Glt_{Ph}, an EAAT homologue from *Pyroccocus horikoshii*, reveals a trimeric bowl-shaped architecture with an aqueous basin facing the extracellular solution and reaching halfway across the membrane bilayer (Supplementary Fig. S1a)[13]. Each protomer harbours eight transmembrane segments, two re-entrant helical hairpins, and independent substrate translocation pathways[14,15]. The first six transmembrane segments form a distorted 'amino-terminal cylinder' and provide all interprotomer contacts, whereas transmembrane segments TM7 and TM8, together with hairpins HP1 and HP2, coalesce to form a highly conserved core within the amino-terminal cylinder.

Nestled between the tips of HP1 and HP2, within a site secluded from aqueous solution, is non-protein electron density that we have previously suggested to represent a bound substrate, the identity of which was not known at the time of the initial structure determination[13]. The location of this buried substrate site is reminiscent of the occluded location of the leucine site in LeuT[16], which is unrelated in amino acid sequence[5]. The structures of both Glt_{Ph} and LeuT indicate that the reaction cycle of these secondary transporters might involve at least three states: open to the outside, occluded, and open to the inside. Here we determine the conformational transitions of the Glt_{Ph} transporter that allow substrates and ions to reach their binding sites from the extracellular solution, explain the mechanism that couples the opening and closing of the extracellular 'gate' to substrate, ion and inhibitor binding, and show that Glt_{Ph} and LeuT share a common sodium-ion-binding motif.

Substrate and ion specificity

Glt_{Ph} from *Pyrococcus horikoshii* shares as much as 36% amino acid sequence identity with the eukaryotic EAATs and exhibits much greater conservation in regions of functional importance[17–23]. Radiolabelled flux experiments revealed that Glt_{Ph} preferentially catalyses the sodium-dependent uptake of ^{3}H-aspartate over ^{3}H-glutamate (Fig. 1a, and Supplementary Fig. S1b). Sodium was overwhelmingly the most effective at driving transport, with lithium supporting very slow uptake (Supplementary Fig. S1b) and potassium yielding no measurable transport activity (data not shown). Aspartate uptake was only modestly stimulated by conditions of an internal negative

[1]Department of Biochemistry and Molecular Biophysics, and [2]Howard Hughes Medical Institute, Columbia University, 650 West 168th Street New York, New York 10032, USA. [3]Suntory Institute for Bioorganic Research, Wakayamadai, Shimamoto-cho, Misima-gun, Osaka 618-8503, Japan. †Present addresses: Department of Physiology and Biophysics, Weill Medical College of Cornell University, 1300 York Avenue, New York, New York 10021, USA (O.B.); National Institute of Neurological Disorders and Stroke, National Institutes of Health, 35 Convent Drive, Bethesda, Maryland 20892, USA (R.M.R.); Department of Biological Sciences, Purdue University, West Lafayette, Indiana 47907, USA (D.Y.); Vollum Institute and Howard Hughes Medical Institute, Oregon Health and Science University, Portland, Oregon 97239, USA (E.G.).
*These authors contributed equally to this work.

potential (Fig. 1a); therefore, although indicative, this does not provide conclusive evidence of electrogenic transport. Strikingly, D,L-threo-β-benzyloxyaspartate (TBOA; Supplementary Fig. S1c), a competitive inhibitor of eukaryotic glutamate transporters[24], inhibited aspartate uptake with a 50% inhibitory concentration (IC_{50}) of 3.3 ± 1.5 μM (mean ± s.d.) (Fig. 1a, and Supplementary Fig. S1d).

To measure substrate and ion binding to Glt_{Ph}, we developed a fluorescence-based assay by introducing a single tryptophan residue (L130W; Supplementary Fig. S1a). Upon titration of Glt_{Ph}-L130W with L-aspartate, we observed a substantial increase in intrinsic protein fluorescence; from these data we calculated dissociation constant (K_d) values for L-aspartate and D-aspartate of about 1 nM and 10 nM in 200 mM NaCl, respectively (Fig. 1b). In agreement with the uptake experiments, titration of Glt_{Ph}-L130W with aspartate in the presence of potassium, choline and ammonium did not yield significant changes in tryptophan fluorescence. Lithium (Li^+) supported aspartate binding, although the K_d measured in the presence of 200 mM LiCl was about 1,000-fold higher than that measured in 200 mM NaCl. In contrast to aspartate, glutamate bound only weakly to Glt_{Ph} (Fig. 1c); this bacterial homologue therefore differs from the mammalian EAATs, which transport L-glutamate, L-aspartate and D-aspartate with apparent micromolar affinities[25–27].

To define the position of aspartate in the substrate-binding site we exploited the fact that L-cysteine sulphinic acid (L-CS; Fig. 1c and Supplementary Fig. S1c) binds tightly to Glt_{Ph} and harbours an anomalous scatterer (sulphur), thereby allowing us to position the sulphinic moiety in anomalous difference Fourier maps derived from cocrystals of Glt_{Ph} and L-CS. Together with simulated annealing omit maps calculated from aspartate-bound crystals, we fitted aspartate into its sausage-shaped electron density by assuming that the β-carboxylate of aspartate occupied the same position as the sulphinic acid group of L-CS (Supplementary Fig. S2b, c and Supplementary Table S1).

Aspartate is completely buried within a polar chamber located halfway across the membrane bilayer and formed by the tips of HP1 and HP2, the unwound region of TM7 (NMDGT motif) and polar residues of amphipathic TM8, regions previously implicated in substrate binding and translocation[28]. Key interactions involve the α-amino and carboxylate groups of aspartate and R276 (HP1), V355 (HP2) and D394/N401 (TM8) as well as the β-carboxylate and T314 (TM7), G359 (HP2) and R397 (TM8). Residues involved in aspartate coordination (Fig. 1d) are mostly conserved, with notable substitutions of D394, which is close to the α-amino group and is a serine residue in dicarboxylate transporters[29,30] and R397, which is proximal to the β-carboxylate and is a neutral amino acid or an aspartate in neutral amino acid transporters of eukaryotes[31,32] and bacteria[9,33], respectively.

Extracellular gate

The occluded substrate-binding site observed in Glt_{Ph} raises the question of how aspartate reaches this site from the extracellular or intracellular solution, and what portions of the transporter act as gates, controlling access to the binding site. A clue to the identity of the extracellular gate came from solving the crystal structure of Glt_{Ph} in complex with the non-transportable blocker TBOA (Supplementary Fig. S1c). The overall structure of the transporter is similar in the

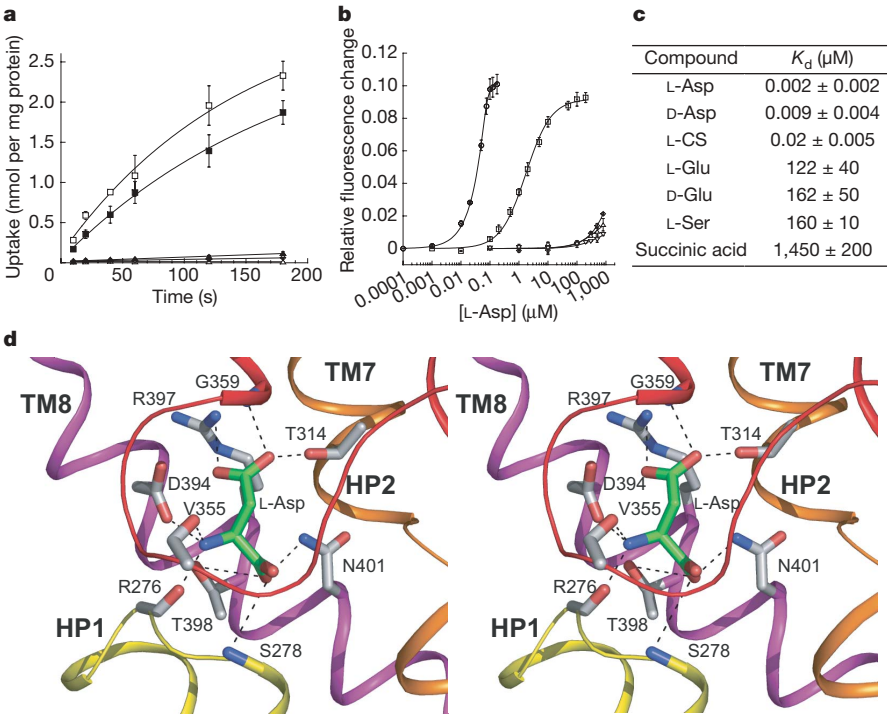

Figure 1 | Glt_{Ph} is an aspartate-specific sodium-driven transporter. **a**, Ion specificity and inhibition of ^{3}H L-aspartate uptake by Glt_{Ph}. Loaded proteoliposomes were diluted into solutions containing the following ions (in mM; see Methods; initial rates are in parentheses): 100 Na^+, 200 K^+ (filled squares, 14 pmol mg s^{-1}); 100 Na^+, 200 choline, internal negative (open squares, 20 pmol mg s^{-1}); 100 Li^+, 200 K^+ (diamonds, 0.1 pmol mg s^{-1}); 100 Na^+, 200 K^+, 1 mM TBOA (filled triangles, 0.5 pmol mg s^{-1}); and 100 choline, 200 K^+ (open triangles, −0.04 pmol mg s^{-1}). **b**, Fluorescence changes observed in the Glt_{Ph}-L130W mutant on titration with L-aspartate in the presence of the chloride salts of the following ions (each at 200 mM): Na^+ (circles), Li^+ (squares), K^+ (diamonds), NH_4^+ (triangles) and choline (inverted triangles). Uptake experiments with the L130W mutant show that it is active, although the level of activity is about 15-fold lower than for the wild-type transporter (Supplementary Fig. S1a). **c**, Dissociation constants for potential substrates in 200 mM NaCl. **d**, Stereo view of the aspartate-binding site showing HP1 (yellow), TM7 (orange), HP2 (red) and TM8 (magenta). A remarkable number of polar contacts solvate the highly charged substrate and include interactions with D394, main-chain carbonyls of R276 (HP1) and V355 (HP2), the amide nitrogen of N401 (TM8), the hydroxyl of T398 (TM8), the main-chain nitrogen of S278, the guanidinium group of R397 (TM8), the hydroxyl of T314 (TM7) and the main-chain nitrogen of G359 (HP2). Results in **a**–**c** are means ± s.d.

aspartate-bound and TBOA-bound complexes with the important exception of two regions: in the TBOA-bound structure HP2 adopts an 'open' conformation, moving as much as 10 Å from its position in the aspartate-bound complex towards the 3L4 loop, with the 3L4 loop also shifting closer to HP2, enabling direct contacts (Fig. 2a, and Supplementary Fig. S3b).

Guided by anomalous difference maps calculated from diffraction data of the complex with 3-bromo-TBOA (3-Br-TBOA), we modelled TBOA into the excess electron density observed in Glt_{Ph}–TBOA density maps (Fig. 2a, and Supplementary Fig. S3a). We found that the aspartate moiety of TBOA binds in the substrate-binding site, in harmony with the observation that TBOA has competitive inhibition kinetics[24] and that the bulky benzyl group lodges against the tip of HP2, propping it in an open conformation. The benzyl group contacts HP2 near the main-chain atoms of G359 and interacts with M311 in TM7. The conservation of M311 provides a structural explanation for the broad yet potent inhibition by TBOA of eukaryotic glutamate transporters and of the evolutionarily distant Glt_{Ph}.

The movement of HP2 in the TBOA-bound complex exposes the substrate-binding site to the extracellular solution (Fig. 2a, c) and raises the question whether HP2 adopts an 'open' conformation before aspartate binding when the transporter is in the 'apo' state. We prepared substrate-depleted Glt_{Ph} crystals (see Methods) and examined threefold averaged electron density maps corresponding to the HP2 region. We found that HP2 predominantly occupies an 'open' conformation, essentially indistinguishable from that seen in the TBOA-bound state (Fig. 2b). In unaveraged maps, however, subunit C and to a smaller degree subunit A showed density for HP2 in a closed conformation, perhaps because of residual aspartate, lattice interactions or stochastic fluctuation of HP2. Nevertheless, these results indicate that in the absence of substrate, HP2 can adopt an 'open' conformation, rendering the substrate-binding site accessible to extracellular solution (Fig. 2c).

Closure of HP2, as seen in the aspartate-bound state, creates a crevice between HP2, the 3L4 loop and TM4a (Fig. 2d). In all three subunits an elongated electron density feature is observed in this crevice, extending from the solvent-filled basin to the outer, lipid-exposed 'walls' of the transporter and lying nearly parallel to the membrane plane (Supplementary Fig. S3c–e); we have modelled this feature as the alkyl chain of a lipid molecule. Identification of a state-dependent lipid binding pocket in Glt_{Ph} indicates that similar pockets might exist in eukaryotic transporters, perhaps providing sites for lipid binding and the modulation of transporter activity[34].

Sodium coupling

In a manner similar to substrate transport by the EAATs[35], transport of aspartate by Glt_{Ph} is sodium dependent. Fluorescence binding assays with Glt_{Ph}-L130W revealed that aspartate binding itself was sodium dependent. At sodium concentrations above 50 mM, the K_d values for aspartate were lower than the protein concentrations used in the assays, resulting in binding isotherms that were anomalously steep (see Supplementary Information). At lower sodium concentra-

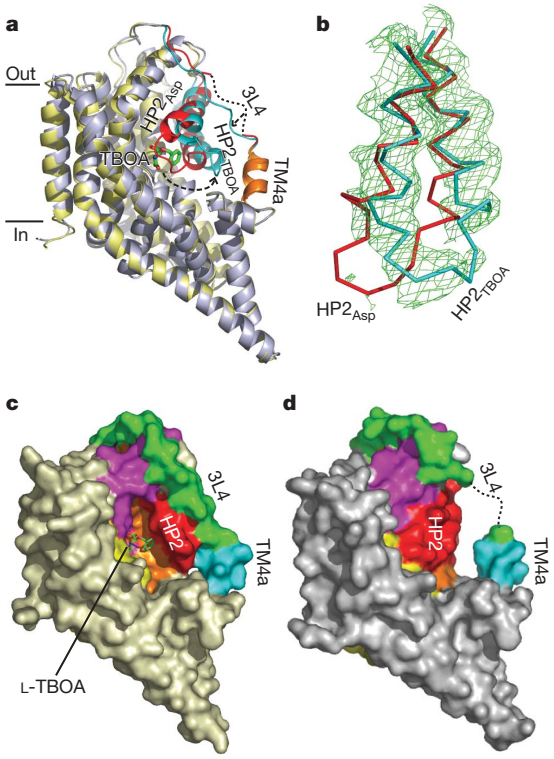

Figure 2 | HP2 is the extracellular gate. **a**, Overlay of Glt_{Ph}–L-Asp (grey) and Glt_{Ph}–TBOA (gold) complexes. Single protomers are shown in a schematic representation and the regions undergoing significant conformational changes are in red (L-aspartate complex) and in cyan (TBOA complex). TM4a is orange. The model of TBOA is shown in stick representation. **b**, Simulated annealing $2F_o - F_c$ omit electron density map for HP2 in apo Glt_{Ph} (green mesh; 1σ). α-Carbon traces for HP2 in the L-aspartate (red) and TBOA (cyan) complexes are shown. **c**, **d**, Solvent-accessible surface view of a single subunit in complex with TBOA (**c**) and with aspartate (**d**); the 3L4 loop, TM7, HP1, HP2 and TM8 are coloured as in Supplementary Fig. S1a. In **d** the 'gap' between HP2 and 3L4/TM4a is partly filled with lipid (see also Supplementary Fig. S3c–e).

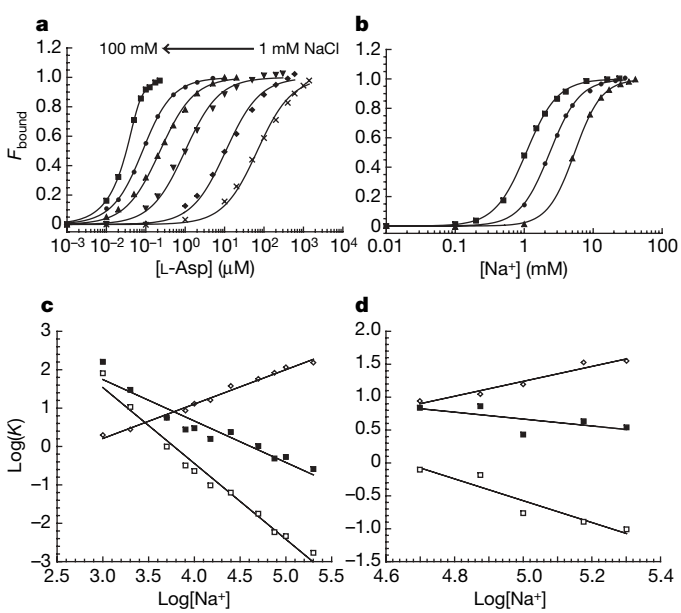

Figure 3 | Binding of ligands and sodium to Glt_{Ph}. **a**, **b**, Sodium dependence of L-aspartate binding (**a**) and L-aspartate dependence of sodium binding (**b**; triangles, 1 μM; circles, 10 μM; squares, 100 μM L-Asp). The fraction of bound transporter was calculated by dividing the relative fluorescence change of Glt_{Ph}-L130W on the addition of L-aspartate or sodium by the total change at the end of the titration. Endpoint sodium concentrations are shown above the graph. Solid lines through the data are fits to the equations described in the Supplementary Information. **c**, Logarithmic plots of L-aspartate K_d values (open squares; slope = -2.0 ± 0.1) and TBOA K_i values (filled squares; slope = -1.1 ± 0.1) against log([Na^+](μM)) are shown for Glt_{Ph}-L130W, with data from the fluorescence assay. Differences between log K_d values for L-aspartate and log K_i values for TBOA (diamonds; slope = 0.9 ± 0.03) are also plotted. **d**, Logarithmic plots of L-aspartate (open squares; slope = -1.7 ± 0.3) and sodium (filled squares; slope = -0.3 ± 0.3) concentrations from fluorescence binding studies of the Glt_{Ph}-D405N/L130W mutant. Differences between log K_d values for L-aspartate and log K_i values for TBOA (diamonds; slope = 1.1 ± 0.15) are also plotted.

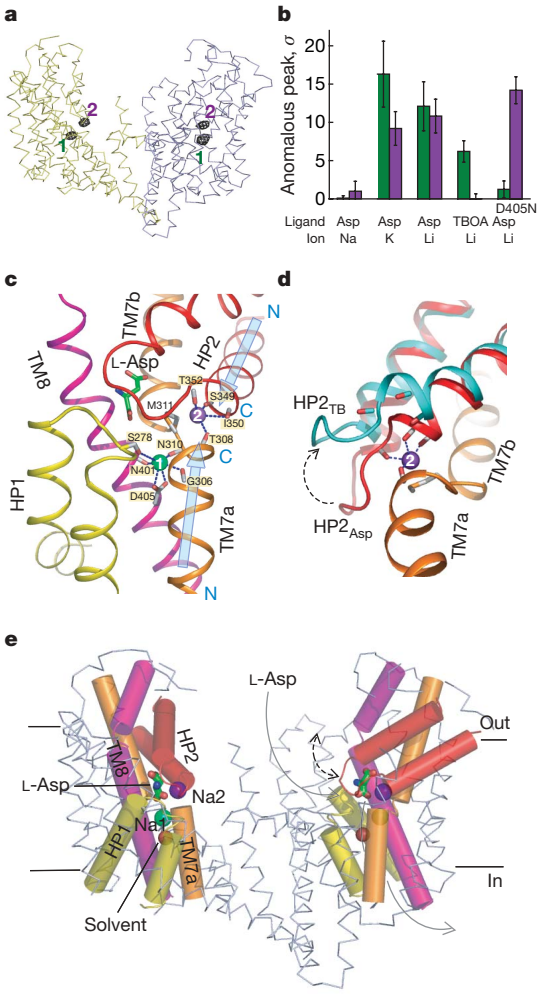

Figure 4 | Sodium-binding sites in Glt_{Ph}. **a**, Two subunits of Glt_{Ph} are shown. Anomalous difference Fourier map calculated for Glt_{Ph}–L-aspartate complex crystals soaked in 50 mM Tl^+ and 100 mM Li^+ and contoured at 5.5σ (black mesh). Two ion-binding sites are designated 1 (green) and 2 (purple). **b**, Heights of peaks on anomalous difference maps for crystals soaked in 50 mM Tl^+ and 100 mM Na^+, K^+ or Li^+. Peaks are mean values derived from the three protomers and one (Na^+) or two (K^+, Li^+) data sets. Anomalous peaks for TBOA-bound Glt_{Ph} and aspartate-bound D405N soaked in Tl^+ and Li^+ are also shown. When no clear peaks were detected on the map, values of the electron density at sites 1 or 2 were employed. The green bars represent the peak heights at site 1 and the purple bars the peak heights at site 2. Results are means ± s.d. **c**, Oxygen atoms that are within 3.5 Å of the sodium ions are labelled and connected to the sodium ions by dashed lines. Light blue arrows represent the dipole moments of helices TM7a and HP2a. **d**, Opening of HP2 observed in the TBOA-bound structure destroys sodium site 2. The dashed arrow indicates the direction of HP2 motion in the TBOA-bound state. Sodium bound at site 2 in aspartate-bound Glt_{Ph} is shown as a sphere, with coordinating oxygen interactions depicted by dashed lines. **e**, Location of sodium-binding sites on the permeation pathway of aspartate. Two protomers of Glt_{Ph} are shown. N-terminal cylinders are in ribbon representation, the TM helices in the C-terminal protein cores are shown as cylinders and bound aspartate is shown in stick representation. HP2 (red) serves as an extracellular gate and opens to afford aspartate access to the binding site. Sodium 2 (purple) serves as a lock on the gate, providing additional energy necessary for its closure. Below the substrate-binding site is sodium 1 (green) and bound solvent (red sphere). The proposed intracellular gate is formed by HP1 (yellow), TM7 (orange) and TM8 (magenta), which are held together by sodium 1. The proposed permeation pathway for the substrate is shown as a grey line and motions of HP2 are shown as a dashed double-headed arrow.

tions, however, aspartate bound less tightly and the isotherms were well fitted with the Hill equation with coefficients near unity, suggesting that aspartate binds independently to each protomer (Fig. 3a)[14]. Measurements of aspartate binding to wild-type Glt_{Ph} by isothermal titration calorimetry (ITC) yielded similar results, reinforcing the conclusion that aspartate binding is not cooperative (Supplementary Fig. S4a).

Sodium titrations of Glt_{Ph}-L130W in the presence of aspartate also resulted in fluorescence changes, and yielded apparent K_d values for sodium in the millimolar range and Hill coefficients of about 2, suggesting the coupled binding of at least two sodium ions (Fig. 3b). A plot of log aspartate K_d against log sodium concentration was well fitted by a straight line with a slope of about 2, which corresponds to the number of sodium ions coupled to the binding of an aspartate molecule (Fig. 3c, Supplementary Fig. S4c and Supplementary Information). Measurements from ITC experiments yielded similar K_d values and slopes between 1.6 and 2.0, providing further support for the conclusion that each subunit independently binds one aspartate and at least two sodium ions.

The sodium dependence of TBOA binding, by contrast, was weaker, and plotting the apparent inhibition constants (K_i) for TBOA as a function of sodium concentration yielded linear fits with slopes of about 1.1 (Fig. 3c). Here, competition experiments with aspartate were performed because titration of TBOA with unliganded Glt_{Ph}-L130W did not yield a fluorescence signal. In ITC experiments with wild-type Glt_{Ph} (Supplementary Fig. S4b, c) we also found that TBOA binding was coupled to about one sodium ion. The ITC experiments yielded K_d values that were severalfold lower than the K_i values from the fluorescence experiments, and this might have been due to unfavourable interactions between HP2 in the open state and the tryptophan residue in L130W-Glt_{Ph} (Supplementary Fig. S3b). Nevertheless, these two independent approaches show that TBOA binding is coupled to about one sodium ion, whereas aspartate binding is coupled to about two.

Sodium-binding sites

To define the positions of the sodium sites in Glt_{Ph} we employed thallium(I) (Tl^+), a monovalent ion with a robust anomalous scattering signal. Examination of anomalous difference Fourier maps of crystals soaked in thallous nitrate revealed two strong peaks per subunit (Fig. 4a), resulting from the partial occupancy (about 0.2–0.4) of Tl^+ at these sites. To evaluate whether these sites, defined as sites 1 and 2, were specific for sodium, competition experiments were performed by soaking crystals of the Glt_{Ph}–aspartate complex in solutions containing Tl^+ and either Li^+, Na^+ or K^+ (Fig. 4b). Only sodium diminished the thallium anomalous density peaks, supporting the contention that the sites labelled by thallium are genuine sodium sites. We suggest that lithium did not compete with Tl^+ simply because the binding of Li^+ is about 10–30-fold weaker than sodium, as estimated from the ~1,000-fold weaker binding of aspartate in the presence of Li^+ (Fig. 1b). Similar crystallographic studies of the Glt_{Ph}–TBOA complex revealed only one strong Tl^+ peak in anomalous difference Fourier maps (Fig. 4b), located at site 1.

The sodium sites are near the bound aspartate, although neither is in direct contact (Fig. 4c). Sodium site 1 is buried deeply within the protein, below aspartate, and is coordinated by three carbonyl oxygens in TM7 and TM8, a carboxyl group of D405 in TM8 and possibly by a hydroxyl oxygen of S278 in HP1. Sodium 2 is buried just under HP2 and seems to have only four coordinating carbonyl oxygens located in TM7 and HP2. The carboxy termini of helices TM7a and HP2a point towards site 2, indicating that their dipole moments might stabilize the bound ion (Fig. 4c). Involvement of HP2 in the formation of site 2 explains why this site is absent in the TBOA-bound state: HP2 is no longer proximal to TM7a and therefore cannot contribute coordinating oxygen atoms (Fig. 4d).

Why does Tl^+ label the sodium sites in Glt_{Ph}? The Pauling radius of Tl^+ ($r = 1.40$ Å) is most similar to that of K^+ ($r = 1.33$ Å) and

substantially larger than that of Na^+ ($r = 0.95$ Å), and Tl^+ is typically employed as a heavy-ion analogue of potassium, although even in complexes with crown ethers Tl^+ and K^+ often form completely different structures[36]. Tl^+ is a highly polarizable ion, and we suggest that it forms favourable interactions with the sulphur of M311, which is sandwiched between the sodium-binding sites, 3.3–5.0 Å from the sodium ion positions (Fig. 4c). Thus, in addition to the oxygen ligands that define the smaller sodium-selective binding sites, Tl^+, but not K^+, is able to exploit the presence of M311 and bind to these sodium-selective sites. Although Tl^+ did not support ^{3}H-aspartate uptake in flux experiments, Tl^+ can replace sodium in the binding of aspartate to Glt_{Ph}, in a similar manner to Li^+, and Tl^+ reversibly inhibited Na^+-driven aspartate transport (Supplementary Fig. S5).

D405N mutant

The carboxylate group of D405 coordinates sodium 1 (Fig. 4c) and, whereas it is conserved in mammalian orthologues, it is an asparagine residue in some bacterial proton-dependent transporters[9]. To probe the role of D405 in sodium binding and in its coupling to aspartate binding, we made the D405N mutant and performed crystallographic and binding studies. The crystal structure of the Glt_{Ph}-D405N–aspartate complex was indistinguishable from that of the wild-type Glt_{Ph}–aspartate complex. However, on inspection of anomalous Fourier difference maps calculated from data measured on crystals soaked in Tl^+, we found a strong peak at site 2 but no peak at site 1 (Fig. 4b), suggesting that the mutation weakened the binding of Tl^+, and by analogy that of Na^+, to site 1. The D405N mutation diminished aspartate binding about 100-fold, resulting in a K_d of about 100 nM in 200 mM NaCl (data not shown).

Substrate and inhibitor binding was still sodium dependent, and logarithmic plots of aspartate K_d and TBOA K_i values against sodium concentration gave straight lines with slopes of 1.7 and 0.5, respectively (Fig. 3d). In agreement with the loss of Tl^+ binding to site 1, the sodium dependence for aspartate and TBOA binding to the D405N mutant was decreased. Because the apparent couplings were decreased by 0.3–0.5 rather than by about 1.0, we suggest that the binding of sodium to site 1 is only partly coupled to aspartate and TBOA binding and that there may be a third sodium site, one that is resistant to Tl^+ substitution. A recent study on the EAAC1 glutamate transporter indicates that the mutation equivalent to D405N in eukaryotic transporters does not abrogate sodium binding to the glutamate-free state[37] and is also consistent with one or more additional sodium binding sites.

TM7 harbours a sodium-binding motif

We compared the sodium sites in Glt_{Ph}, together with key elements of the local protein structure, with the sodium sites identified in LeuT (PDB code 2A65). Strikingly, key unwound transmembrane segments of Glt_{Ph} (TM7) and LeuT (TM1)[16] reveal similarity in their local protein conformations and in the relative disposition of sodium-binding sites (Fig. 5a–c). In Glt_{Ph} and LeuT, sodium site 1 is defined, in part, by coordinating carbonyl oxygen atoms occupying nearly equivalent positions, and the ion in site 2 is also coordinated by an equivalently positioned carbonyl oxygen atom. Even though Glt_{Ph} and LeuT are unrelated in amino acid sequence and three-dimensional structure, elements of protein structure surrounding the sodium sites are somewhat similarly organized (Fig. 5d, e). For example, TM8 in both Glt_{Ph} and LeuT fits into a groove created by the unwound portions of TM7 and TM1, respectively, and in so doing it provides key coordinating oxygen atoms to sodium site 1. Elaboration of sodium site 2, in turn, is provided by exposed carbonyl oxygen atoms at the C termini of two roughly equivalently positioned helices, which are HP2 in Glt_{Ph} and TM6 in LeuT.

Taken together, the similarities in local protein structure and coordination of the sodium sites in Glt_{Ph} and LeuT indicate that sodium dependent transporters might possess a common sodium-ion-binding motif, as exemplified by TM7 and TM1 in Glt_{Ph} and LeuT. This motif has the following features (Fig. 5c): first, a break in helix structure of three to five residues that opens up the peptide chain to permit sodium ion coordination by main-chain carbonyl oxygen atoms; second, a site 1 defined by carbonyl oxygen atoms occupying the first and fourth (LeuT) or fifth (Glt_{Ph}) positions of the motif; and third, a site 2 defined by the carbonyl oxygen atom at the third position. This motif not only satisfies the requirements for sodium ion coordination but also provides a mechanism by which ion binding and unbinding can be coupled to local and long-distance conformational changes through the bending and twisting of the associated helical elements.

Mechanism

A synthesis of the structural and biophysical experiments described here, together with previous studies on glutamate transporters[38], allows us to propose a mechanism for coupling sodium and aspartate binding, movement of HP2, and inhibition of transport by TBOA

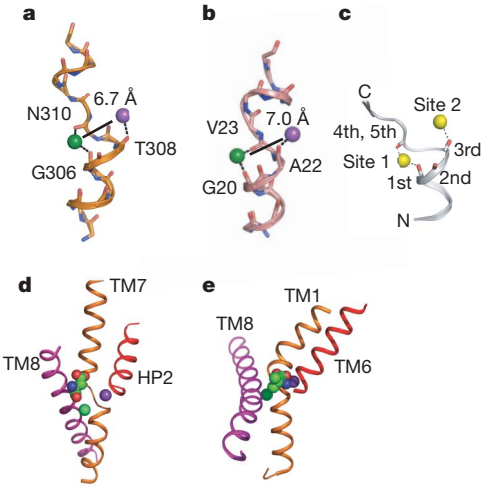

Figure 5 | Sodium-binding motif. **a**, TM7 of Glt_{Ph}, showing ions at sites 1 and 2, coloured according to Fig. 4c. **b**, TM1 of LeuT and sodium ions 1 (green) and 2 (purple). **c**, The unwound region of Glt_{Ph} TM7 defines a monovalent-ion-binding motif in sodium-dependent transporters. **d**, **e**, Substrate, sodium ions and key transmembrane regions of Glt_{Ph} (**d**) and LeuT (**e**).

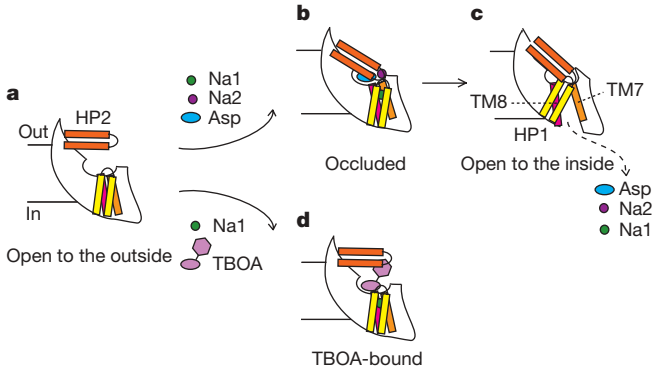

Figure 6 | Schematic mechanism illustrated by a diagram of a single subunit. **a**, Apo state with HP2 in an open conformation. **b**, Sodium ions 1 and 2 and aspartate bind and induce closure of HP2, yielding the occluded state. **c**, Opening of the internal gate allows the release of aspartate and sodium to the cytoplasm and may involve the movement of HP1, TM7 and TM8. In this state, HP2 may form additional interactions with the protein core, stabilizing HP2 in a closed conformation. **d**, TBOA binding blocks transport by stabilizing HP2 in an open conformation and precluding the binding of sodium to site 2.

(Fig. 6). Beginning with the apo state, we suggest that sodium ions bind to sites 1 and 2, together with aspartate binding to the substrate site, and that these binding events are tightly coupled to each other and induce the closure of HP2. Inhibition of transport by TBOA occurs because TBOA blocks HP2 in an open conformation, preventing sodium from binding to site 2 and halting further conformational changes along the transport cycle.

The location of the sodium sites relative to aspartate and to portions of the transporter that are either known to move during transport (HP2)[15,20,21,39–41] or that are likely to rearrange but have not yet been proved to do so, is highly suggestive (Fig. 4e). We note that site 1 is 'below' aspartate, located closer to the cytoplasm, whereas site 2 is 'above' aspartate, and nearer to the extracellular solution. Site 2 has a key function in stabilizing the extracellular gate (HP2) in a closed conformation, and we suggest that site 1 might similarly stabilize a closed conformation of the intracellular gate. Although the composition of the intracellular gate is unknown, HP1, TM7a and TM8 are likely to be important. Indeed, between sodium site 1 and the cytoplasmic surface of the transporter, in both the aspartate-bound and TBOA-bound structures, we find excess, non-protein, electron density occluded in a pocket between HP1, TM7a and TM8 (Fig. 4e), which we interpret as trapped solvent. On further conformational changes, this solvent-filled cavity may expand and provide a pathway for aspartate and sodium to reach the cytoplasm, probably along the polar face of TM8.

We speculate that there is a mechanistically symmetrical relation between sodium site 2/HP2 and sodium site 1/HP1. As we have shown that site 2 is coupled to the opening and closing of HP2, site 1 may be coupled to the opening and closing of HP1 and other components of the cytoplasmic gate (Fig. 6), thus providing a mechanism for the sodium-coupled alternating access to the aspartate-binding site and elevating sodium ions to essential 'gate-keepers' of Glt_{Ph} and other members of this sodium-coupled transporter family.

METHODS

Ligand and ion binding. Glt_{Ph} and Glt_{Ph}-L130W were expressed as His_8 fusion proteins and purified as described previously[13]. Proteins were concentrated and dialysed against HEPES/Tris buffer, pH 7.4, containing 200 mM choline chloride, 1 mM NaCl and 1 mM n-dodecyl-β-D-maltoside. For fluorescence assays Glt_{Ph}-L130W was diluted about 200-fold (final protein concentration about 100 nM) at 20 °C into a 3-ml quartz cell containing buffer with variable NaCl concentrations. Tryptophan fluorescence was excited at 295 nm and emission was measured at 334 nm. Fluorescence changes were normalized for the initial protein fluorescence, and binding isotherms were analysed as described in Supplementary Information. For ITC experiments Glt_{Ph} was diluted to 4 μM into the reaction cell of a Microcal VP-ITC calorimeter and titrations were performed at 20 °C by injecting 3–5 μl of syringe solution containing potassium salts of L-aspartic acid (100 μM) or L-TBOA (125 μM). Binding isotherms were analysed with Microcal software.

Transport assay. Liposomes were prepared with *Escherichia coli* polar lipid extract and egg phosphatidylcholine in a 3:1 (w/w) ratio. Preformed liposomes were treated with Triton X-100 at a 2:1 (w:w) lipid to detergent ratio, and Glt_{Ph} was reconstituted at a protein-to-lipid ratio of 1:330 (w/w). Transport was assayed at 30 °C (ref. 42). Typically, the uptake reaction was initiated by diluting proteoliposomes loaded with 20 mM HEPES/Tris buffer pH 7.4, 200 mM KCl and 100 mM choline chloride into buffer containing 20 mM HEPES/Tris pH 7.4, 200 mM KCl, 100 mM XCl ($X = Na^+$, Li^+, K^+ or Ch^+), 1 μM valinomycin and 75 nM L-^{3}H-aspartate or 75 nM L-^{3}H-glutamate. Background was defined as the counts observed when the proteoliposomes were diluted into the buffer with which they were loaded. To test the electrogenicity of transport, KCl in the uptake buffer was replaced by choline chloride (inside negative). TBOA dose–response measurement was performed in the presence of 75 nM L-^{3}H-aspartate and uptake was performed for 3 min. For Tl^+ experiments, liposomes were loaded with 100 mM potassium methanesulphonate, 20 mM HEPES pH 7.4, and all external salts were nitrate salts. Uptake was performed for 4 min at 30 °C. Reported values are means of at least three independent experiments and the uncertainties are the standard error of the mean.

Crystallography. The heptahistidine mutant of Glt_{Ph} (CAT7) and the CAT7-D405N mutant were expressed, purified and crystallized as described previously[13] in the presence of L-Glu, L-Asp or D-Asp or in the absence of substrates. In some cases the protein solution was supplemented with *E. coli* total lipid extract at a final concentration of about 0.1 mM before crystallization. To obtain crystals of TBOA-bound, 3-Br-TBOA-bound or L-CS-bound CAT7, protein purified in the presence of 5 mM L-Glu was supplemented with 1 mM TBOA before crystallization. Crystals were then soaked in mother liquor supplemented with 25% poly(ethylene glycol) (PEG)1000 and either 1 mM TBOA, 10 mM 3-Br-TBOA or 5 mM L-CS. In ion replacement experiments, CAT7 crystals were soaked in 25% PEG1000, 100 mM MES/Tris pH 6.0, 5 mM substrate, 2 mM n-decyl-β-D-maltoside and either 100 mM X_2SO_4 ($X = Li^+$, Na^+ or K^+) and 50 mM $TlNO_3$ or 150 mM Li_2SO4.

Diffraction data sets were indexed, integrated and scaled using the HKL-2000 package (Supplementary Table S1)[43]. Further analysis was performed with CCP4 programs[44]. Initial phases for the NAT crystal (Supplementary Table S1) were determined by rigid-body refinement in REFMAC[44] using published CAT7 coordinates (PDB code 1XFH). Phases for TB were obtained similarly, except that residues 110–130 and 337–371 were deleted from the model. Phases were further improved by rounds of manual rebuilding followed by restrained refinement in REFMAC with tight three-fold NCS restraints. A large peak on the $F_o - F_c$ and $2F_o - F_c$ difference maps in the core of the protein was modelled as a single water molecule. During the last round the restrained refinement was run with six TLS groups defined as three protomers and three substrate or TBOA molecules. Phases for all other crystals except NA and LID405N were obtained by rigid-body refinement. All electron density maps were subjected to threefold real-space averaging with RAVE software[45], except in ion competition experiments in which the heights of the anomalous peaks were determined separately in each protomer and then averaged.

Data for NA crystals, soaked in 50 mM $TlNO_3$ and 100 mM NaCl, were used to model sodium ions. There were no peaks on the anomalous difference Fourier maps, suggesting that thallium ions were replaced by sodium. In contrast, there were clear peaks on the $F_o - F_c$ and $2F_o - F_c$ maps, which were used to place sodium ions manually. The protein model with ions was further refined as described above. To estimate Tl^+ occupancies, the occupancy of the Tl^+ ions was manually adjusted, followed by threefold NCS-restrained refinement of *B*-factors, and this process was repeated several times until the *B*-factors of the Tl^+ ions were similar to those of the surrounding protein atoms.

To prepare apo crystals, CAT7 was purified and crystallized in the absence of the externally added substrate but in the presence of sodium, which is required for sustained protein stability. Under these conditions, CAT7 crystallizes in complex with a putative substrate carried over from bacterial growth medium. Repetitive soaking of crystals in solutions devoid of sodium is required to induce dissociation of the bound substrate and to produce an apo state. Although crystals prepared in this manner were of diminished quality, they were isomorphous to the aspartate complex. During data analysis HP2 was excluded from the protein model and, after rigid-body refinement, we performed real-space three-fold averaging to improve the quality of the maps, and subsequently inspected averaged and unaveraged maps.

Received 5 July; accepted 15 November 2006.
Published online 17 January 2007.

1. Hille, B. *Ion Channels of Excitable Membranes* (Sinauer Associates, Sunderland, Massachusetts, 2001).
2. Läuger, P. *Electrogenic Ion Pumps* (Sinauer Associates, Sunderland, Massachusetts, 1991).
3. Quick, M. W. (ed.) *Transmembrane Transporters* (Wiley-Liss, Hoboken, New Jersey, 2002).
4. Sobczak, I. & Lolkema, J. S. Structural and mechanistic diversity of secondary transporters. *Curr. Opin. Microbiol.* **8,** 161–167 (2005).
5. Chen, N. H., Reith, M. E. & Quick, M. W. Synaptic uptake and beyond: the sodium- and chloride-dependent neurotransmitter transporter family SLC6. *Pflugers Arch.* **447,** 519–531 (2004).
6. Wright, E. M. & Turk, E. The sodium/glucose cotransport family SLC5. *Pflugers Arch.* **447,** 510–518 (2004).
7. Wilson, T. H. & Ding, P. Z. Sodium-substrate cotransport in bacteria. *Biochim. Biophys. Acta* **1505,** 121–130 (2001).
8. Grewer, C. & Rauen, T. Electrogenic glutamate transporters in the CNS: molecular mechanism, pre-steady-state kinetics, and their impact on synaptic signaling. *J. Membr. Biol.* **203,** 1–20 (2005).
9. Slotboom, D. J., Konings, W. N. & Lolkema, J. S. Structural features of the glutamate transporter family. *Microbiol. Mol. Biol. Rev.* **63,** 293–307 (1999).
10. Kanner, B. I. & Bendahan, A. Binding order of substrates to the sodium and potassium ion coupled L-glutamatic acid transporter from rat brain. *Biochemistry* **21,** 6327–6330 (1982).
11. Zerangue, N. & Kavanaugh, M. P. Flux coupling in a neuronal glutamate transporter. *Nature* **383,** 634–637 (1996).
12. Levy, L. M., Warr, O. & Attwell, D. Stoichiometry of the glial glutamate transporter GLT-1 expressed inducibly in a Chinese hamster ovary cell line selected for low

endogenous Na^+-dependent glutamate uptake. *J. Neurosci.* **18,** 9620–9628 (1998).
13. Yernool, D., Boudker, O., Jin, Y. & Gouaux, E. Structure of a glutamate transporter homologue from *Pyrococcus horikoshii*. *Nature* **431,** 811–818 (2004).
14. Grewer, C. *et al.* Individual subunits of the glutamate transporter EAAC1 homotrimer function independently of each other. *Biochemistry* **44,** 11913–11923 (2005).
15. Koch, H. P. & Larsson, H. P. Small-scale molecular motions accomplish glutamate uptake in human glutamate transporters. *J. Neurosci.* **25,** 1730–1736 (2005).
16. Yamashita, A., Singh, S. K., Kawate, T., Jin, Y. & Gouaux, E. Crystal structure of a bacterial homologue of Na^+/Cl^--dependent neurotransmitter transporters. *Nature* **437,** 215–223 (2005).
17. Grunewald, M., Bendahan, A. & Kanner, B. I. Biotinylation of single cysteine mutants of the glutamate transporter GLT-1 from rat brain reveals its unusual topology. *Neuron* **21,** 623–632 (1998).
18. Slotboom, D. J., Lolkema, J. S. & Konings, W. N. Membrane topology of the C-terminal half of the neuronal, glial, and bacterial glutamate transporter family. *J. Biol. Chem.* **271,** 31317–31321 (1996).
19. Seal, R. P. & Amara, S. G. A reentrant loop domain in the glutamate carrier EAAT1 participates in substrate binding and translocation. *Neuron* **21,** 1487–1498 (1998).
20. Slotboom, D. J., Sobczak, I., Konings, W. N. & Lolkema, J. S. A conserved serine-rich stretch in the glutamate transporter family forms a substrate-sensitive reentrant loop. *Proc. Natl Acad. Sci. USA* **96,** 14282–14287 (1999).
21. Grunewald, M. & Kanner, B. I. The accessibility of a novel reentrant loop of the glutamate transporter GLT-1 is restricted by its substrate. *J. Biol. Chem.* **275,** 9684–9689 (2000).
22. Slotboom, D. J., Konings, W. N. & Lolkema, J. S. Cysteine-scanning mutagenesis reveals a highly amphipathic, pore-lining membrane-spanning helix in the glutamate transporter GltT. *J. Biol. Chem.* **276,** 10775–10781 (2001).
23. Grunewald, M., Menaker, D. & Kanner, B. I. Cysteine-scanning mutagenesis reveals a conformationally sensitive reentrant pore-loop in the glutamate transporter GLT-1. *J. Biol. Chem.* **277,** 26074–26080 (2002).
24. Shimamoto, K. *et al.* DL-threo-β-benzyloxyaspartate, a potent blocker of excitatory amino acid transporters. *Mol. Pharmacol.* **53,** 195–201 (1998).
25. Kanner, B. I. & Schuldiner, S. Mechanism of transport and storage of neurotransmitters. *CRC Crit. Rev. Biochem.* **22,** 1–38 (1987).
26. Nicholls, D. & Attwell, D. The release and uptake of excitatory amino acids. *Trends Pharmacol. Sci.* **11,** 462–468 (1990).
27. Arriza, J. L. *et al.* Functional comparisons of three glutamate transporter subtypes cloned from human motor cortex. *J. Neurosci.* **14,** 5559–5569 (1994).
28. Slotboom, D. J., Konings, W. N. & Lolkema, J. S. Glutamate transporters combine transporter- and channel-like features. *Trends Biochem. Sci.* **26,** 534–539 (2001).
29. Engelke, T., Jording, D., Kapp, D. & Pühler, A. Identification and sequence analysis of the *Rhizobium meliloti dctA* gene encoding the C_4-dicarboxylate carrier. *J. Bacteriol.* **171,** 5551–5560 (1989).
30. Yurgel, S. N. & Kahn, M. L. *Sinorhizobium meliloti dctA* mutants with partial ability to transport dicarboxylic acids. *J. Bacteriol.* **187,** 1161–1172 (2005).
31. Shafqat, S. *et al.* Cloning and expression of a novel Na^+-dependent neutral amino acid transporter structurally related to mammalian Na^+/glutamate cotransporters. *J. Biol. Chem.* **268,** 15351–15355 (1993).
32. Arriza, J. L. *et al.* Cloning and expression of a human neutral amino acid transporter with structural similarity to the glutamate transporter family. *J. Biol. Chem.* **268,** 15329–15332 (1993).
33. Ogawa, W., Kim, Y.-M., Mizushima, T. & Tsuchiya, T. Cloning and expression of the gene for the Na^+-coupled serine transporter from *Escherichia coli* and characteristics of the transporter. *J. Bacteriol.* **180,** 6749–6752 (1998).
34. Zerangue, N., Arriza, J. L., Amara, S. G. & Kavanaugh, M. P. Differential modulation of human glutamate transporter subtypes by arachidonic acid. *J. Biol. Chem.* **270,** 6433–6435 (1995).
35. Kanner, B. I. & Sharon, I. Active transport of L-glutamate by membrane vesicles isolated from rat brain. *Biochemistry* **17,** 3949–3953 (1978).
36. Mudring, A.-V. & Rieger, F. Lone pair effect in thallium(I) macrocyclic compounds. *Inorg. Chem.* **44,** 6240–6243 (2005).
37. Tao, Z., Zhang, Z. & Grewer, C. Neutralization of the aspartic acid residue Asp-367, but not Asp-454, inhibits binding of Na^+ to the glutamate-free form and cycling of the glutamate carrier EAAC1. *J. Biol. Chem.* **281,** 10263–10272 (2006).
38. Kanner, B. I. & Borre, L. The dual-function glutamate transporters: structure and molecular characterization of the substrate binding sites. *Biochim. Biophys. Acta* **1555,** 92–95 (2002).
39. Zarbiv, R., Grunewald, M., Kavanaugh, M. P. & Kanner, B. I. Cysteine scanning of the surroundings of an alkali-ion binding site of the glutamate transporter GLT-1 reveals a conformationally sensitive residue. *J. Biol. Chem.* **273,** 14231–14237 (1998).
40. Zhang, Y. & Kanner, B. I. Two serine residues of the glutamate transporter GLT-1 are crucial for coupling the fluxes of sodium and the neurotransmitter. *Proc. Natl Acad. Sci. USA* **96,** 1710–1715 (1999).
41. Brocke, L., Bendahan, A., Grunewald, M. & Kanner, B. I. Proximity of two oppositely oriented reentrant loops in the glutamate transporter GLT-1 indentified by paired cysteine mutagenesis. *J. Biol. Chem.* **277,** 3985–3992 (2002).
42. Gaillard, I., Slotboom, D. J., Knol, J., Lolkema, J. S. & Konings, W. N. Purification and reconstitution of the glutamate carrier GltT of the thermophilic bacterium *Bacillus stearothermophilus*. *Biochemistry* **35,** 6150–6156 (1996).
43. Otwinowski, Z. & Minor, W. Processing of X-ray diffraction data collected in oscillation mode. *Methods Enzymol.* **276,** 307–326 (1997).
44. CCP4 Project. N. The *CCP4* suite: programs for protein crystallography. *Acta Crystallogr. D* **50,** 760–763 (1994).
45. Kleywegt, G. J. Use of non-crystallographic symmetry in protein structure refinement. *Acta Crystallogr. D* **52,** 842–857 (1996).

Supplementary Information is linked to the online version of the paper at www.nature.com/nature.

Acknowledgements We thank J. Mindell for support, and B. Hille and R. MacKinnon for constructive criticism. X-ray diffraction data were measured at beamlines X4A and X29 at the National Synchrotron Light Source and 8.2.2 at the Advanced Light Source. This work was supported by a National Research Service Award postdoctoral fellowship (D.Y.) and by the National Institutes of Health (E.G). E.G. is an Investigator with the Howard Hughes Medical Institute.

Author Information The coordinates for the lithium-bound native (NAT), TBOA-bound (TB) and sodium-bound (NA) states are deposited in the Protein Data Bank under accession codes 2NWL, 2NWW and 2NWX, respectively. Reprints and permissions information is available at www.nature.com/reprints. The authors declare no competing financial interests. Correspondence and requests for materials should be addressed to E.G. (gouauxe@ohsu.edu).